

On Collisionless Electron-Ion Temperature Equilibration in the Fast Solar Wind

J. Martin Laming¹

ABSTRACT

We explore a mechanism, entirely new to the fast solar wind, of electron heating by lower hybrid waves to explain the shift to higher charge states observed in various elements in the fast wind at 1 A.U. relative to the original coronal hole plasma. This process is a variation on that previously discussed for two temperature accretion flows by Begelman & Chiueh. Lower hybrid waves are generated by gyrating minor ions (mainly α -particles) and become significant once strong ion cyclotron heating sets in beyond $1.5R_{\odot}$. In this way the model avoids conflict with SUMER electron temperature diagnostic measurements between 1 and $1.5R_{\odot}$. The principal requirement for such a process to work is the existence of density gradients in the fast solar wind, with scale length of similar order to the proton inertial length. Similar size structures have previously been inferred by other authors from radio scintillation observations and considerations of ion cyclotron wave generation by global resonant MHD waves.

1. Introduction

The 1990 October launch of Ulysses and the subsequent polar passes in late 1994, 1995, 2000 and 2001 have provided a wealth of new data and insights concerning solar polar coronal holes and the fast solar wind emanating from them. The south polar pass of 1994 (during solar minimum) highlighted a particular problem concerning the charge states observed in various elements in the fast wind, which are generally characteristic of higher temperatures than observed spectroscopically in coronal holes. Coronal holes show very little emission in spectral lines corresponding to plasma temperatures of 10^6 K or greater (e.g. Doschek & Feldman 1977; David et al. 1998; Wilhelm et al. 1998), whereas Geiss et al. (1995) find

¹E. O Hulbert Center for Space Research, Naval Research Laboratory, Code 7674L, Washington DC 20375

jlaming@ssd5.nrl.navy.mil

freeze-in temperatures from the O, Si and Fe charge states in the range $1.2 - 1.5 \times 10^6$ K. Fe in the fast solar wind is dominated by charge states Fe^{10+} and Fe^{11+} , whereas lines from Fe X, XI, and XII are generally not detectable in spectroscopy of coronal holes; an old result going back to Doschek & Feldman (1977). Geiss et al. (1995) and Ko et al. (1997) recognized that the electron temperature must increase outwards as the fast wind flows out of the coronal hole, and were able to derive an empirical temperature profile, but did not specify a mechanism to produce such an effect.

The heuristic temperature profile of Ko et al. (1997) predicts a maximum in the electron temperature of about 1.5×10^6 K relatively close to the solar surface, at about $1.5R_\odot$ heliocentric distance. However observations in a temperature diagnostic line ratio in Mg IX (Wilhelm et al. 1998) out to $1.6R_\odot$ with the SUMER instrument on SOHO failed to detect such a temperature increase. Consequently, in a series of papers (Esser & Edgar 2000, 2001; Chen, Esser, & Hu 2003), the effects of a halo electron distribution (i.e. a power law tail on the core Maxwellian) that remains consistent with SUMER electron temperature measurements and differential flows between ions of the same element were investigated. While carefully chosen differential flows can explain most of the in situ charge state observations without the need for extra electron heating, the required speed differentials are so large as to be implausible, leaving electron heating as the most likely explanation. The fast solar wind is often observed (at 1 AU) with $T_{e\parallel} > T_{e\perp}$ (Feldman et al. 1975) and with $T_{e\parallel}/T_{e\perp} > T_{p\parallel}/T_{p\perp}$, and this electron temperature anisotropy can be described in term of a core Maxwellian distribution and a halo higher temperature Maxwellian or power law distribution, which contains typically 5% of the electrons (Marsch 1991). It has been suggested that this halo distribution persists all the way back to the sun (Esser & Edgar 2000), and this might be appealing since the electron temperature diagnostic used by Wilhelm et al. (1998) (Mg IX) belongs to an isoelectronic sequence that is in general insensitive to such a population (Keenan 1984), whereas the ionization balance is not. However the O VI diagnostic used by David et al. (1998) should be sensitive to suprathermal electrons but shows no evidence of their existence out to $1.3 R_\odot$. In any case, it seems that such an explanation must fail, because the halo distribution will transfer energy to the core Maxwellian by Coulomb collisions on a timescale $\sim (10^7 - 10^8) \times T_{e6}^{3/2}/n_e$ s, (T_{e6} is the electron temperature in 10^6 K, and n_e is the electron density in cm^{-3}) and even with the fastest inferred outflow speeds, the solar wind would not get very far before a discernable increase in the core Maxwellian electron temperature should become apparent.

2. Wave Acceleration and Heating in the Fast Solar Wind

The acceleration of the fast solar wind is widely believed to occur through ion cyclotron waves, though the manner in which they are excited remains controversial. The original concept, that low frequency waves alone are sufficient to accelerate the fast solar wind to its eventual speed of 700-800 km s⁻¹, appears to be adequate for acceleration of protons but not for the minor ions (Ofman & Davila 2001), which in this case would be accelerated mainly by the Coulomb drag of the protons. Hence minor ions should flow out of the coronal hole with lower speeds than the protons. Renewed indications that ion cyclotron waves are required come from the UVCS Doppler dimming measurements of the O⁵⁺ outflow velocity, which are *large* compared to hydrogen, $\sim 300 - 400$ km s⁻¹ at 2.5-3.0 R_{\odot} heliocentric distance. By contrast a purely low frequency wave driven outflow would produce O⁵⁺ outflow velocities of less than 100 km s⁻¹ at this distance. Similar indications come from the observation in the fast solar wind of faster flow speeds for α particles (and in fact all minor ions) than for protons with Ulysses and Helios (Reisenfeld et al. 2001; von Steiger et al. 2000; Neugebauer et al. 1996). The Ulysses and Helios observations only go in to the sun as far as $\sim 1.4R_{\odot}$ heliocentric distance, but the inference that α particles flow out from the sun at least as fast as protons in the fast solar wind may be extended to lower altitudes by spectroscopic observations with SUMER of the He abundance (Laming & Feldman 2003). Here He abundances at or below the usual fast solar wind value of 5% relative to H are found, implying flow speeds at these lower altitudes at or above the H flow speed to keep the flux of α particles constant. This is also consistent with recent modelling by Li (2003), where by heating primarily the α particles, a steep transition region, hot corona and fast wind can be created by high frequency Alfvén waves propagating up from the coronal base. On the other hand Cranmer, Field, & Kohl (1999) and Cranmer (2000) argue that the high frequency (or ion cyclotron) waves that accelerate the fast wind must be generated throughout the extended corona, due to their rapid dissipation once generated, and the observation that ions continue to be heated in the range $1.5 - 5R_{\odot}$ heliocentric distance.

We propose an entirely new (to the fast wind; though see Schwartz, Feldman, & Gary 1981, for related considerations) means of heating/accelerating electrons. At a heliocentric distance between 1.5 and 2 R_{\odot} , the perpendicular *velocities* of the minor ions start to exceed those of the protons (e.g. Cranmer et al. 1999). There are also indications from observations that α particles are similarly heated. All these ions will have significantly larger gyroradii than the protons. In the presence of a density gradient, these ions may then excite lower hybrid waves in the colder protons. This requires that the electron gyroradius be less than the wavelength/2 π . The waves will damp by heating electrons in a direction parallel to the magnetic field. Unless other restrictions set in, the waves ultimately will saturate once the electrons are heated such that their gyroradii are no longer sufficiently small. In the

region of interest the plasma conditions are approximately magnetic field $B = 1$ G and density $n_e = 10^6$ cm $^{-3}$. Then the proton and electron gyrofrequencies are $\Omega_p = 10^4$ and $\Omega_e = 1.8 \times 10^7$, and the lower hybrid frequency is $\Omega_{LH} = \sqrt{\Omega_p \Omega_e} = 4 \times 10^5$ (all in rad s $^{-1}$). The electron and proton plasma frequencies are $\omega_{pe} = 6 \times 10^7$ and $\omega_{pp} = 1.5 \times 10^6$. It will turn out that waves are excited at low k by ions moving with velocities greater than the proton thermal speed, so the limit $\omega \gg \sqrt{2}kv_i$ of the plasma dispersion function is appropriate, and that α particles will be species most important for the wave generation. This is due to their large gyroradius compared to protons and their high abundance compared to other minor ions.

Lower hybrid waves are electrostatic ion oscillations, which can occur in magnetic fields strong enough that the electron gyroradius is smaller than the lower hybrid wavelength/2 π . Due to this necessary magnetization of the electrons, the waves propagate preferentially across magnetic field lines. The parallel component of the wavevector $k_{\parallel}/k < \omega_{pi}/\omega_{pe}$. Since $\omega/k_{\perp} \sim (m_e/m_i)^{1/2} \omega/k_{\parallel}$ the wave can simultaneously be in resonance with ions moving across the magnetic field and electrons moving along magnetic field lines, which facilitates collisionless energy exchange between ions and electrons on timescales much faster than that associated with Coulomb collisions. They have also been discussed in connection with cometary X-ray emission, electron acceleration in solar flares, supernova remnant shock waves and Advection Dominated Accretion Flows (ADAFS) (Vaisberg et al. 1983; Krinosel'skikh et al. 1985; Bingham et al. 1997; Shapiro et al. 1999; Bingham et al. 2000; Begelman & Chiueh 1988; Luo, Wei, & Feng 2003; McClements et al. 1997), and observed in situ together with accelerated electrons at Halley's comet (Gringauz et al. 1986; Klimov et al. 1986). A cold plasma theory for lower-hybrid waves is given in the Appendix of Laming (2001a). Here we summarize the theory with finite electron and ion temperatures.

The dispersion relation is (see e.g Laming 2001b)

$$\omega^2 = \frac{\omega_{pe}^2 \left(I k_{\parallel}^2 / k^2 \right) / (1 + \omega_{pe}^2 / c^2 k^2)}{1 + \frac{\omega_{pi}^2}{k^2 v_i^2} \left(1 - \phi \left(\frac{\omega}{\sqrt{2}kv_i} \right) \right) + \frac{\omega_{pe}^2}{k^2 v_e^2} (1 - I)} \quad (1)$$

where $I = \frac{m_e}{k_B T_e} \int_0^{+\infty} J_0^2 \left(\frac{k_{\perp} v_{\perp}}{\Omega_e} \right) \exp \left(\frac{-m_e v_{\perp}^2}{2k_B T_e} \right) v_{\perp} dv_{\perp}$, $v_e^2 = k_B T_e / m_e$ and $v_i^2 = k_B T_i / m_i$, and $\phi(z) = -z/\sqrt{\pi} \int_{-\infty}^{\infty} \exp(-t^2) / (t - z) dt$ is the usual plasma dispersion function ($T_{e,i}$ and $m_{e,i}$ are electron and ion temperatures and masses respectively and k_B is Boltzmann's constant). Specializing to $\omega \gg \sqrt{2}kv_i$ and $\Omega_e \gg k_{\perp} v_{e\perp}$, so that $I \simeq 1 - k_{\perp}^2 v_{e\perp}^2 / \Omega_e^2$ and $\phi \simeq 1 + i\sqrt{\pi/2}(\omega/kv_i) \exp(-\omega^2/2k^2v_i^2)$ and taking $\omega_{pe} \gg \Omega_e$ and $c \rightarrow \infty$,

$$\omega = \Omega_e \frac{k_{\parallel}}{k} \left[1 - \frac{\Omega_e^2}{2\omega_{pe}^2} - \frac{i}{2} \sqrt{\frac{\pi}{2}} \frac{\omega \Omega_e^2 \omega_{pi}^2}{k^3 v_i^3 \omega_{pe}^2} \exp(-\omega^2/2k^2v_i^2) + \dots \right]. \quad (2)$$

The instability is illustrated schematically in Figure 1. The density is increasing towards the right, and the density gradient is perpendicular to the magnetic field. A local anisotropy in the ion distribution develops in the direction formed by the cross product of density gradient and magnetic field, which in the representation of Figure 1 is into or out of the page. This is similar to a scenario envisaged by Begelman & Chiueh (1988), who were interested in electron-ion equilibration in two temperature accretion flows. We consider the effect of a density gradient in a uniform magnetic field. In such a situation the ion distribution function is given by

$$f(v_i) = \frac{m_i}{2\pi k_B T_{i\perp}} \sqrt{\frac{m_i}{2\pi k_B T_{i\parallel}}} (1 - v_{iy}/\Omega_i L) \exp \left(-\frac{m_i v_{iz}^2}{2k_B T_{i\parallel}} - \frac{m_i (v_{ix}^2 + v_{iy}^2)}{2k_B T_{i\perp}} \right), \quad (3)$$

where the magnetic field $\vec{B} = B\vec{z}$, and the density gradient $(dn/dx)\vec{x}$ is related to L by $n(dx/dn) = L$. We consider the growth of lower hybrid waves in the protons excited by minor ions with large gyroradii. The growth rate for each minor ion species is given by (Laming 2001a)

$$\begin{aligned} \gamma_i &= \frac{Afq^2}{M} \frac{\pi}{2} \frac{\omega^3}{nk^2} \left(1 + \frac{\omega_{pe}^2}{\omega_{pi}^2} \cos^2 \theta \right)^{-1} \int \vec{k} \cdot \frac{\partial f_i}{\partial \vec{v}_i} \delta^3 \left(\omega - \vec{k} \cdot \vec{v}_i \right) d^3 \vec{v}_i \\ &= \frac{Afq^2}{M} \frac{\omega}{2} \sqrt{\frac{\pi}{2}} \left(\frac{\omega}{kv_{th\perp}} \right)^3 \left(1 + \frac{\omega_{pe}^2}{\omega_{pi}^2} \cos^2 \theta \right)^{-1} \left[\frac{\omega}{k\Omega_i L} - 1 - \frac{kv_{th\perp}^2}{\omega\Omega_i L} \right] \exp \left(-\frac{\omega^2}{2k^2 v_{th\perp}^2} \right), \end{aligned} \quad (4)$$

where θ is the angle between \vec{B} and \vec{k} , $v_{th\perp} = \sqrt{k_B T_{i\perp}/m_i}$ and Afq^2/M is the product of the element abundance, ionization fraction and charge squared of the particular ions that excite the wave, divided by their mass in atomic mass units. Protons are expected to have insufficiently large gyroradii to excite lower-hybrid waves, and so the factor Afq^2/M favors α -particles over other minor ions in the wave generation. The term -1 in the square brackets represents the ion Landau damping given by the imaginary part of the expression for ω in equation 2. Equation 4 is similar to equation (3.20) in Begelman & Chiueh (1988), with the identification of their drift velocity $v_{di} = -v_{th\perp}^2/\Omega_i L$, and in their case $\omega/k \ll v_{th\perp}$. Their treatment yields waves at much higher k than ours does, since they consider a single ion distribution drifting with velocity v_{di} producing waves at $k \simeq \omega/v_{di}$, whereas we treat the effect at a single point of a continuum of different Maxwellians with differing densities (but otherwise the same) producing waves at $k \simeq (\omega/v_{th\perp})(r_g/L)$. This difference is appropriate in view of the fact that they are interested in plasmas with ion pressure \gg magnetic pressure \gg electron pressure where the plasma itself amplifies the magnetic field, while here we are concerned with magnetic pressure \gg ion and electron pressures where the magnetic field is imposed externally. Begelman & Chiueh (1988) also considered the effects of magnetic curvature. We assume that the necessary gradients in magnetic field are much less likely to exist in the low β plasma of the solar coronal hole. We find the wavevector k_{max} where

the growth rate is maximized in the direction perpendicular to \vec{B} (i.e. $\theta = \pi/2$), and the maximum growth rate itself, which is plotted in units of $\omega \times Afq^2/M$ in Figure 2.

If the waves are driven to marginal stability $k_{max} \simeq \Omega_e/v_{e\perp} \simeq \omega r_g/Lv_{i\perp}$, where $v_{i\perp}$ is the perpendicular ion velocity, equation 1 can be written

$$v_{e\perp}^2 = \frac{\Omega_e^2 v_{i\perp}^2 \left(1 + (1 - I) \omega_{pe}^2/k^2 v_{e\perp}^2\right) \left(1 + \omega_{pe}^2/c^2 k^2\right) L^2}{\omega_{pe}^2 I \left(k_{\parallel}^2/k^2\right) + \omega_{pp}^2 \left(1 + \omega_{pe}^2/c^2 k^2\right)} \frac{L^2}{r_g^2}. \quad (5)$$

At saturation where $k_{\perp} v_{e\perp}/\Omega_e \simeq 1$, $I \simeq 1/2$, and putting $k_{\parallel}/k = \cos \theta$,

$$v_{e\perp}^2 = \frac{\Omega_e^2 v_{i\perp}^2 \left(1 + \omega_{pe}^2/2\Omega_e^2\right) \left(1 + \omega_{pe}^2 v_{e\perp}^2/\Omega_e^2 c^2\right) L^2}{\left(\omega_{pe}^2 \cos^2 \theta\right)/2 + \omega_{pp}^2 \left(1 + \omega_{pe}^2 v_{e\perp}^2/\Omega_e^2 c^2\right)} \frac{L^2}{r_g^2}. \quad (6)$$

This is a quadratic equation for $v_{e\perp}^2$ which has lowest order solution

$$v_{e\perp}^2 \simeq \frac{\omega_{pe}^2 v_{i\perp}^2}{2\omega_{pp}^2} \left(1 + \frac{\omega_{pe}^2}{2\omega_{pp}^2} \cos^2 \theta\right)^{-1} \frac{L^2}{r_g^2}. \quad (7)$$

The kinetic growth rate varies as $\gamma \propto \left(1 + \frac{\omega_{pe}^2}{\omega_{pp}^2} \cos^2 \theta\right)^{-1}$, (Laming 2001a) and averaging $v_{e\perp}^2$ over this growth rate gives $\langle v_{e\perp}^2 \rangle = v_{i\perp}^2 (1 - 1/\sqrt{2}) \omega_{pe}^2 L^2 / \omega_{pp}^2 r_g^2$. Thus in principle electron and ion temperatures can equilibrate (assuming that $(1 - 1/\sqrt{2}) L^2 / r_g^2 > 1$), in the sense that the waves do not saturate before this is achieved.

3. Solar Wind Ionization Balance Models

We use an adaptation of the BLASPHEMER (BLASt Propagation in Highly EMitting EnviRonment)² code (Laming 2001b; Laming & Grun 2002, 2003; Laming & Hwang 2003), which follows the time dependent ionization balance and temperatures of a Lagrangian plasma parcel as it expands in the solar wind. The density n_{iq} of ions of element i with charge q is given by

$$\frac{dn_{iq}}{dt} = n_e (C_{ion,q-1} n_{i,q-1} - C_{ion,q} n_{iq}) + n_e (C_{rr,q+1} + C_{dr,q+1}) n_{i,q+1} - n_e (C_{rr,q} + C_{dr,q}) n_{iq} \quad (8)$$

where $C_{ion,q}$, $C_{rr,q}$, $C_{dr,q}$ are the rates for electron impact ionization, radiative recombination and dielectronic recombination respectively, out of the charge state q . These rates are the

²The name gives away its origin in modelling laboratory and astrophysical shock waves.

same as those used in the recent ionization balance calculations of Mazzotta et al. (1998), using subroutines kindly supplied by Dr P. Mazzotta (private communication 2000). The electron density n_e is determined from the condition that the plasma be electrically neutral. The ion and electron temperatures, T_{iq} and T_e are coupled by Coulomb collisions by

$$\frac{dT_{iq}}{dt} = -0.13n_e \frac{(T_{iq} - T_e)}{M_{iq} T_e^{3/2}} \frac{q^3 n_{iq} / (q+1)}{\left(\sum_{iq} n_{iq}\right)} \left(\frac{\ln \Lambda}{37}\right) - \frac{4}{3} \frac{\gamma_{iq} U_w}{n_q k_B} \quad (9)$$

and

$$\frac{dT_e}{dt} = \frac{0.13n_e}{T_e^{3/2}} \sum_{iq} \frac{(T_{iq} - T_e)}{M_{iq}} \frac{q^2 n_{iq} / (q+1)}{\left(\sum_{iq} n_{iq}\right)} \left(\frac{\ln \Lambda}{37}\right) - \frac{T_e}{n_e} \left(\frac{dn_e}{dt}\right)_{ion} - \frac{2}{3n_e k_B} \frac{dQ}{dt} + \sum_{iq} \frac{4}{3} \frac{\gamma_{iq} U_w}{n_e k_B}. \quad (10)$$

Here M_{iq} is the atomic mass of the ions of element i and charge q in the plasma, and $\ln \Lambda \simeq 28$ is the Coulomb logarithm. The term in dQ/dT represents plasma energy losses due to ionization and radiation. Radiation losses can be taken from Summers & McWhirter (1979), though are generally negligible in applications to the solar wind. The term $-(T_e/n_e)(dn_e/dt)_{ion}$ gives the reduction in electron temperature when the electron density increases due to ionization. Recombinations, which reduce the electron density, do not result in an increase in the electron temperature in low density plasmas, since the energy of the recombined electron is radiated away (in either radiative or dielectronic recombination), rather than being shared with the other plasma electrons as would be the case for three-body recombination in dense plasmas.

The last terms in equations 9 and 10 represent collisionless ion-electron energy transfer, which we estimate assuming that the population of lower hybrid waves is approximately steady state. Then the wave growth rate due to the gyrating ions is equal to the wave Landau damping rate due to the electrons, and the energy transfer rate is given by $2\gamma_i U_w$ in ergs $\text{cm}^{-3}\text{s}^{-1}$ where $U_w = E_0^2/8\pi$ is the wave energy density in terms of the wave peak electric field E_0 . A threshold electric field for lower hybrid waves between the linear and stochastic regimes has been determined by Karney (1978) by numerical integration of the Hamiltonian equations of motion, and also analytically using an ion trapping argument, to be

$$E_{thr} = \frac{1}{4} \left(\frac{\Omega_p}{\omega}\right)^{1/3} \frac{\omega}{kc} B_0, \quad (11)$$

where B_0 is the background magnetic field and Ω_p is the proton gyrofrequency. This field marks the onset of proton heating as well as electron heating by the waves. We take $E_0 = E_{thr}$ (probably a conservative assumption). Writing the electron heating rate in terms of both collisional and collisionless processes, with $T_i \gg T_e$ and dropping the q subscript in

specializing to one ion species alone,

$$\frac{dT_e}{dt} \simeq 0.13n_e \frac{q^2/(q+1)}{M_i} \frac{T_i n_i}{T_e^{3/2} n_H} \left(\frac{\ln \Lambda}{37} \right) + \frac{\gamma_i}{n_e} \frac{B_0^2}{64\pi} \left(\frac{\Omega_p}{\omega} \right)^{2/3} \frac{T_i}{m_i c^2} \frac{\omega^2}{k_{max}^2 v_{iy}^2} \quad (12)$$

where k_{max} is the wavevector where the growth rate is maximized, and $T_i = 2T_{i\perp}/3 = m_i v_{i\perp}^2/3 = 2m_i v_{iy}^2/3$ since $v_{i\perp}^2 = v_{ix}^2 + v_{iy}^2 = 2v_{iy}^2 \gg v_{i\parallel}^2$. In our calculations we modify $\ln \Lambda$ from its usual value to account for the collisionless energy transfer between α -particles and electrons, its new value being given by

$$\left(\frac{\ln \Lambda}{37} \right)' = \left(\frac{\ln \Lambda}{37} \right) + 6.23 \times 10^5 \frac{T_e^{3/2} B_0^3}{n_e^2} \left(\frac{\gamma_i M_i}{\omega A f q^2} \frac{\omega^2}{k^2 v_{iy}^2} \right), \quad (13)$$

the quantity $\gamma_i M_i / \omega A f q^2$ being plotted in Figure 2. The same value is applied to electron heating by other minor ions, and the original value of $\ln \Lambda$ is kept for proton-electron energy transfer. In the region of the solar wind around $1.5R_\odot$ heliocentric distance, where $T_e \sim 10^6$ K, $B_0 \sim 1$ G, $n_e \sim 10^6$ cm $^{-3}$ and $\gamma' = \gamma_i M_i / \omega A f q^2 (\omega / k v_{iy})^2 \sim 0.1 - 1$ for α -particles of around 5% abundance relative to protons, the electron heating rate is increased typically by factors of order 100 - 1000 over that due solely to Coulomb collisions with ions heavier than H.

We use the analytic model of Banaszkiewicz, Axford & McKenzie (1998) for the magnetic field strength. We take the perpendicular velocity for all ions heavier than H from the empirical model for O VI (model B2; equation 28) in Cranmer et al. (1999) in the range $1.5R_\odot - 3.5R_\odot$. Below this we interpolate between values of 20 km s $^{-1}$ on the solar surface and 84 km s $^{-1}$ at $1.5R_\odot$. The flow speed is linearly interpolated between its initial value at the solar surface and 130 km s $^{-1}$ at $1.7R_\odot$, a value determined by Giordano et al. (2000). Above $1.7R_\odot$ the flow speed is allowed to evolve according the the action of the adiabatic invariant in the diverging magnetic field with the perpendicular velocity specified as above, and above $3.5R_\odot$ the perpendicular velocity is also allowed to evolve in this manner, rather than being determined by the fits in Cranmer et al. (1999). The resulting flow speed is a very good match to the empirical models B1 and B2 in Cranmer et al. (1999), as shown in Figure 3 for various values of the initial flow speed, determined to be in the range 3 - 60 km s $^{-1}$ by various authors (Patsourakos & Vial 2000; Hassler et al. 1999; Wilhelm et al. 2000; Gabriel, Bely-Dubau, & Lemaire 2003). Figure 4 shows the electron density in the simulations for initial flow speeds between 5 and 60 km s $^{-1}$, compared with measurements using a diagnostic line ratio in Si VIII by Doschek et al. (1997) and from UVCS polarization brightness observations given by Cranmer et al. (1999). An initial flow speed of around 10-20 km s $^{-1}$ appears to be the best match to the various observations.

Equations 8-10 are integrated following the solar wind out from an initial position at $1.05R_\odot$ out to around $7R_\odot$ by which time charge states are frozen in. Each model follows H,

He, and one minor ion, C, O, Mg, Si, or Fe in the present work, with fractional abundances 0.83, 0.16 and 0.01 respectively by mass. The initial electron and ion temperatures are 9×10^5 K, which also establish the initial ionization balance. The density at this point is taken to be 10^8 cm $^{-3}$. After each time step in the ionization balance, the densities and electron temperature are modified according to the adiabatic expansion of the solar wind governed by the magnetic field geometry and the wind velocity as specified above.

Figure 5 shows the electron temperature profile resulting from simulations with an initial flow speed of 10 km s $^{-1}$ and various values of the lower hybrid growth rate, which depends on the density gradient assumed. For reference, the temperature measurements of Wilhelm et al. (1998) using the Mg IX 750Å /706Å diagnostic line ratio are also given. The error bar on the points at 1.3 and 1.6 R_\odot are estimated here from the scatter in the points on Figure 8 of Wilhelm et al. (1998). These authors use the atomic physics data of Keenan et al. (1984) to derive a temperature ratio, which is consistent with coronal hole temperatures determined by other authors (e.g. Doschek & Feldman 1977; Doschek et al. 2001). More recent calculations in R-matrix and distorted wave approximations summarized by Landi et al. (2001) give temperatures significantly higher or lower respectively, and are likely due to inaccuracies in these atomic data. We base our coronal hole temperatures on works such as Doschek & Feldman (1977) and Doschek et al. (2001) where the ionization balance is the principal temperature diagnostic, and on the O VI observations of David et al. (1998), whose electron temperature diagnostic depends on much less controversial atomic physics. Even if the absolute temperatures measured by Wilhelm et al. (1998) cannot be interpreted with confidence, as they state in their paper, at least the maximum variation of the electron temperature with distance from the solar surface can be constrained by their observations. Figure 6 shows the electron temperature profiles resulting from using the maximum collisionless energy transfer in Figure 5 and differing initial flow speeds, with the highest temperatures resulting from the slowest initial speeds since more time is available for the plasma electron to be heated and the rate of temperature decrease due to adiabatic expansion is lower.

Figures 7, 8, and 9 show the evolution of the ionization balances of O, Si, and Fe with heliocentric distance. In each case the flow starts at a density of 10^8 electrons cm $^{-3}$ and a temperature of 9×10^5 K. The initial flow speed is 20 km s $^{-1}$ and the electron-ion equilibration parameter is $\gamma' = \gamma_i M_i / \omega A f q^2 (\omega^2 / k^2 v_{iy}^2) = 0.5$. Increased ionization commences at around 1.5 R_\odot , in response to the onset of ion cyclotron heating at this location, and charge states freeze in between 2 and 2.5 R_\odot at the values found in situ by Ulysses (Geiss et al. 1995; Ko et al. 1997).

4. Discussion

4.1. Charge State Distributions

The resulting ionization balances are given in Tables 1-4 for C, O, Mg, Si and Fe respectively. From the C and O ionization balances in Table 1, it is clear than only for values of the parameter $\gamma' = (\gamma_i M_i / \omega A f q^2) (\omega / k v_{iy})^2 \simeq 0.5$ and initial wind speeds of 10-20 does sufficient electron heating occur to bring the modelled charge states into agreement with those observed. Tables 2-4 verify that these conclusions do not change when other elements Mg, Si, and Fe are considered. We will discuss the significance of γ' below. Before doing so we remark on the other salient features of the model. The data of Geiss et al. (1995) come from a high speed stream observed closer to the ecliptic plane than the polar observations of Ko et al. (1997), and so are slightly less highly ionized as would be expected. Even so, both sets of observations for the parameters discussed above agree very well with the modelled charge state fractions for C, O, Si and Fe, at least for the two or three charge states that dominate the distributions. Mg is still observed to be more highly charged than the models predict. However we note that the steady state ionization balance for Mg changes dramatically in the temperature range 9×10^5 K to 1.1×10^6 K (Mazzotta et al. 1998), and so we anticipate that small changes in either the model or the atomic data for Mg would also bring this element into agreement. We find no need to invoke different outward flow speeds for the different elements. C, O, Mg, Si, and Fe all flow at the flow speeds determined from O VI Doppler dimming measurements. This is in contrast with the work of Ko et al. (1997), where heavier ions needed to flow out at successively lower speeds, as would be the case in a thermal conduction driven wind. In addition to a faster outflow, we also model higher electron temperatures, as would be expected since less time is available before freeze-in, and so higher electron temperatures are required to produce the necessary ionization. Even so, the electron temperatures modelled here when extrapolated out to 0.3-1 A.U. are still considerably lower than those measured *in situ* by Helios (Marsch et al. 1989). The inclusion of non-zero thermal conduction (see below) might reduce this discrepancy, but it would seem that the conclusion of (Marsch et al. 1989) that “electron temperature profiles in high-speed streams clearly indicated and even required the existence of heating sources other than the one related to the degradation of the electron heat flux” supports our idea of electron heating. We also remark that Ko et al. (1997) made some different choices of atomic data. In particular their choice of O⁶⁺ ionization rate from Lennon et al. (1988) is lower than the rate adopted here from Mazzotta et al. (1998) by a factor of about 0.7, and elsewhere in the literature (e.g. Moores, Golden, & Sampson 1980; Shull & van Steenberg 1982) rates for this process can be greater than that of Lennon et al. (1988) by nearly a factor of 2. The assessment and validation of atomic data is a huge task, beyond the scope of the

current paper (see e.g. Savin & Laming 2002), but clearly central to further quantitative development along the lines suggested in this paper.

Further variations in the atomic rates involved may come from nonthermal electron distributions. Throughout this paper we have taken a Maxwellian electron distribution, tacitly assuming that the electron-electron collision rate is sufficiently fast to maintain such conditions. We argued above that halo electron distributions are unlikely to exist close to the Sun because of this collisional equilibration, and numerical estimates suggest that only at electron densities $< 10^4 - 10^5 \text{ cm}^{-3}$ could a nonthermal electron distribution produced by lower hybrid waves survive (by equating the collisional equilibration rate with the wind expansion rate). Such densities are only found at or beyond the radial position where ion charge states freeze in, and so nonthermal electrons appear unlikely to produce a significant change to our charge state results, given the other current observational constraints. However lower hybrid waves do appear to be a viable means for producing the electron distributions observed in the fast solar wind.

4.2. Small Scale Structures?

The determination that $\gamma' = \gamma_i M_i / \omega A f q^2 (\omega / k v_{iy})^2 \simeq 0.5 - 1$ is necessary to produce the observed charge states requires the existence of density gradients in the fast wind with scale lengths on the order of the α -particle gyroradius, which is about 0.1 km at $1.5 R_\odot$. Radio scintillation observations demonstrating the existence of such size scales in the solar wind in the ecliptic plane have rather a long history (e.g. Coles & Harmon 1989; Armstrong et al. 1990; Coles et al. 1991). These are found perpendicular to the magnetic field, with larger size scales (typically a factor of 10 within $6 R_\odot$, becoming more isotropic at larger distances) inferred along the radial direction. Coles et al. (1995) inferred values of δn_e^2 in polar regions at solar minimum to be around 1/10 to 1/15 of that observed in equatorial regions, but due to a lack of knowledge of n_e in polar regions, were unable to say anything about the variation of $\delta n_e / n_e$. The density measurements reviewed in this paper indicate electron densities in polar regions a factor of 1/2 to 1/3 of those in equatorial regions, making $\delta n_e / n_e$ in polar regions of similar order to, but still slightly smaller than that in equatorial regions. Absolute values of $\delta n_e / n_e$ in coronal hole regions of interest here have been determined observationally by Ofman et al. (1997) to be from 0.1 to a few times 0.1. This is smaller than the value ~ 1 tacitly assumed here, the consequence of which is discussed further below.

Grall et al. (1997) present more data on the transition from anisotropy inside $5-6 R_\odot$ on scales of order 10 km to isotropy further out, concluding that a real change in the microstructure rather than in Alfvén wave turbulence takes place, again with reference to the ecliptic

plane. Feldman et al. (1996) review these interplanetary scintillation observations together with Ulysses observations to constrain the high speed wind structure near its coronal base, and argue that the plasma is “sufficiently structured to relax through generation of a drift-wave instability that results in electrostatic waves having k -vectors oriented perpendicular to \mathbf{B} ”, which is precisely the motivation for the current work. Grall et al. (1997) go further and show that within $6 R_\odot$ large scale turbulence is isotropic with a Kolmogorov spectrum (structure function \propto scale $^{5/3}$), while smaller scale turbulence shows anisotropy with higher structure functions (\propto scale) than Kolmogorov turbulence would predict. The scale at which this transition takes place which can be interpreted (Woo 1996; Woo & Habbal 1997) as the size of the flux tube in which the wind flows, is inferred to be of order 1 km close to the sun.

In a study of electrostatic ion cyclotron wave generation by global resonant MHD modes, Markovskii (2001) suggests that structures may exist with scales down to the proton inertial length $v_A/\Omega_p = c/\omega_{pp}$, which is of the same order of magnitude as the structures already inferred by Woo (1996); Woo & Habbal (1997), and in terms of particle gyroradii about an order of magnitude larger than our present inference. However our evaluation of the lower hybrid wave growth rate assumed Maxwellian distributions for the minor ions. In the presence of a radiation field interacting with the ions, Hasegawa, Mima & Duong-van (1985) show that a “kappa” distribution may result;

$$f(v) dv = \frac{n}{\sqrt{2\pi}v_{th}} \frac{\Gamma(\kappa+1)}{\kappa^{3/2}\Gamma(\kappa-1/2)} \left[1 + \frac{v^2}{2\kappa v_{th}^2}\right]^{-\kappa}, \quad (14)$$

where $v_{th} = \sqrt{k_B T/m}$ is the thermal velocity, Γ is the usual Gamma Function, and κ is a parameter representing the deviation from a Maxwellian distribution, which is obtained in the limit $\kappa \rightarrow \infty$. Observations of the α -particle distribution function in the high speed solar wind generally give $\kappa \simeq 3 - 6$ (Collier et al. 1996; Chotoo et al. 1998). In Figures 10 and 11 we plot the dimensionless lower hybrid growth rate $\gamma_i M_i / \omega A f q^2$ and the parameter $\gamma' = \gamma_i M_i / \omega A f q^2 (\omega / k v_{iy})^2$ against L/r_g . From Figure 11 it may be seen the for $\kappa = 3$ values of L/r_g up to about 7 give acceptable ionization and for lower κ even higher L/r_g would be tolerable. Protons in a kappa distribution may also be able to contribute to the wave generation, reducing the requirement on L/r_g even more. Given the relatively safe assumption that the κ value for α -particles in the coronal hole is similar to or less than that observed in high speed wind streams at about 1 A.U., we conclude that similar density gradients to those proposed by Markovskii (2001) would provide sufficient lower hybrid wave generation and electron heating to produce the observed ionization states of minor ions in the fast wind. Thus these observations provide further support for the mechanism of ion cyclotron wave generation throughout the extended corona proposed by Markovskii (2001), that of a global resonant MHD mode driving a cross field current in the resonant layer which then excites electrostatic ion cyclotron waves. We have also made rather conservative

assumptions concerning the collisionless ion-electron energy transfer. Higher wave electric fields than given by equation 11 (up to $\sim \omega B_0/kc$) are certainly possible (Karney 1978; Bingham et al. 2003), though as the wave amplitude increases from this point, protons begin to be heated as well as electrons (the *stochastic* regime). Under favorable conditions, the ion heating rate may be similar to the electron heating rate. Thus our estimate of the ion-electron equipartition rate may be an underestimate by as much as an order of magnitude, if the wave electric field can be a factor of a few higher, and the electron Landau damping rate only reduced by a factor 0.5. Fuller discussion of this point is beyond the scope of this paper.

4.3. Thermal Conduction

The approach taken in this paper of following a Lagrangian plasma element out through the solar wind acceleration region neglects thermal conduction. Here we argue that such an approximation is most likely justified. The electron temperature gradient is $\sim 10^{-4}$ K cm $^{-1}$ between 1 and 2 R_\odot and $\sim 10^{-5}$ K cm $^{-1}$ for heliocentric distances greater than $3R_\odot$. The Spitzer-Harm heat flux is then $Q \sim 10^7$ ergs cm $^{-2}$ s $^{-1}$ prior to the temperature maximum (for an initial flow speed of 5 km s $^{-1}$; it is lower for initial speeds of 10 and 20 km s $^{-1}$) directed back towards the sun, and oppositely directed and about an order of magnitude lower once the wind has passed the temperature maximum. The cooling rate of the plasma occupying a length of order R_\odot between 2 and 2 R_\odot heliocentric distance is then ~ 0.6 s $^{-1}$, assuming an average electron density in this region of 10 5 cm $^{-3}$. This cooling rate is much faster than that due to adiabatic expansion, $\sim 10^{-4}$ s $^{-1}$.

However in steep temperature gradients and collisionless plasma the Spitzer-Harm thermal conductivity is not appropriate. We estimate the collisionless heat conduction as follows: Begelman & Chiueh (1988) give the electron velocity diffusion coefficient in the “moderately non-linear regime” (i.e. corresponding to the turbulence level just before ion trapping sets in) as

$$D_{||}(v_e) \simeq \frac{e^2 \langle \delta E_{||}^2 \rangle}{m_e^2 \omega}. \quad (15)$$

Putting $\delta E_{||} = E_0 \sqrt{m_e/2m_i}$ and using equation 11 we find $D_{||} \simeq e^2 v_i^2 B_0^2 / 400 m_e m_i c^2 \omega \simeq 4 \times 10^{17} (v_i/200 \text{km s}^{-1})^2 (\omega/4 \times 10^5 \text{rads}^{-1}) \text{cm}^2 \text{s}^{-3}$. The time taken to accelerate an electron from rest to a parallel velocity $v_{||}$ is $t \sim v_{||}^2 / D_{||}$, which evaluates to ~ 1 s taking $v_{||} = 1.7 \times 10^9$ cm s $^{-1}$, the electron thermal speed at $T_e = 10^7$ K. The electron-electron collision time entering the Spitzer-Harm conductivity is around 3000 s, so in lower-hybrid turbulence the heat conduction rate should be reduced from our former estimate by a factor 1/3000, giving

a cooling rate $2 \times 10^{-4} \text{ s}^{-1}$, which is now comparable with that due to adiabatic expansion. Higher degrees of lower hybrid turbulence (see above) would decrease the conductive cooling rate even further.

That the heat conductivity should be reduced from the Spitzer-Harm value in steep temperature gradients is well known (e.g Bell, Evans & Nicholas 1981; Salem et al. 2003). However our estimate of heat conduction is significantly lower than one would normally predict. Saturated conduction is usually defined as heat conduction where electrons carry their own thermal energy at their thermal speed. The rationale for this is that at faster flow speeds (relative to the ions), a Buneman instability would develop, generating Langmuir waves that would inhibit the heat flow. Applied to the case above, the saturated heat flux would be $\sim 3.5 \times 10^5 \text{ ergs cm}^{-2}\text{s}^{-1}$. In our situation the heat conducting electrons may also excite lower-hybrid waves with a similar threshold drift velocity. In fact we should expect the limiting flux to be lower than this simple estimate, as indeed it is, because in our case not only heat conducting electrons but also ions generate the lower-hybrid turbulence. Any electron heating mechanism invoked to explain the observed charge state distributions in the fast solar wind must require an anomalous thermal conductivity to avoid the deposited heat from being conducted back to the coronal hole, which would conflict with the SUMER temperature diagnostics of Wilhelm et al. (1998) and David et al. (1998). We consider that the heating and anomalous thermal conductivity provided simultaneously by lower-hybrid waves to be a desirable aspect of the model, in that one mechanism provides both features.

5. Summary and Conclusions

In this paper we have argued that a small amount of the energy deposited in ions between 1.5 and $2 R_\odot$ should eventually find its way to the electrons via an instability that generates lower hybrid waves. No attempt has been made to address the ion cyclotron heating problem, other than to show that the density gradients we require are similar to those postulated by Markovskii (2001) to generate electrostatic ion cyclotron waves from a global resonant MHD mode. As such, our line of reasoning is complementary to that in a recent paper by Cranmer & van Ballegooijen (2003). In addressing the larger problem of ion cyclotron heating, these authors speculate that low frequency Alfvén waves can Landau damp on electrons. This parallel heating should produce electron beaming and discrete phase-space holes which may heat ions via stochastic processes. Thus the ion heating derives from the electron energization (by low frequency Alfvén waves), rather than the electron heating deriving from the ion heating as in the picture presented here.

While a number of quantitative issues remain unresolved (atomic data, thermal conduction

tion), we believe that an explanation for the observed fast wind elemental charge states in terms of lower hybrid wave electron heating is certainly plausible, and should be considered along with other possibilities already discussed in the literature (e.g Vocks & Mann 2003). More accurate numerical models would allow us to exploit this interpretation and allow more rigorous investigation of density inhomogeneities in the fast solar wind, with important consequences for the generation of ion cyclotron waves throughout the extended corona. As well as being potentially crucial to our understanding of the acceleration of the fast solar wind, the lower hybrid wave instability is also of interest elsewhere in astrophysics, and the Sun and solar system offer an attractive “laboratory” for the exploration of collisionless plasma physics processes that are otherwise inaccessible to experiment (see e.g. the recent debate on electron-ion equilibration in ADAFs in Binney 2003; Quataert 2003; Pariev & Blackman 2003).

The work was supported by NASA Contract S13783G and by the NRL/ONR Solar Magnetism and the Earth’s Environment 6.1 Research Option. I am grateful to Steven Cranmer for enlightening discussions.

REFERENCES

Armstrong, J. W., Coles, W. A., Kojima, M., & Rickett, B. J. 1990, *ApJ*, 358, 685

Banaszkiewicz, M., Axford, W. I., & McKenzie, J. F. 1998, *A&A*, 337, 940

Begelman, M. C., & Chiueh, T. 1988, *ApJ*, 332, 872

Bell, A. R., Evans, R. G., & Nicholas, D. J. 1981, *Phys. Rev. Lett.*, 46, 243

Bingham, R., Dawson, J. M., Shapiro, V. D., Mendis, D. A., & Kellett, B. J. 1997, *Science*, 275, 49

Bingham, R., Kellett, B. J., Dawson, J. M., Shapiro, V. D., & Mendis, D. A. 2000, *ApJS*, 127, 233

Bingham, R., Kellett, B. J., Cairns, R. A., Tonge, J., & Mendonça, J. T. 2003, *ApJ*, 595, 279

Binney, J. 2003, *MNRAS*, submitted, astro-ph/0308171

Chen, Y., Esser, R., & Hu, Y. 2003, *ApJ*, 582, 467

Chotoo, K., Collier, M. R., Galvin, A. B., Hamilton, D. C., & Gloeckler, G. 1998, *J. Geophys. Res.*, 103, 17441

Coles, W. A., & Harmon, J. K. 1989, *ApJ*, 337, 1023

Coles, W. A., Lui, W., Harmon, J. K., & Martin, C. L. 1991, *JGR*, 96, 1745

Coles, W. A., Grall, R. R., Klinglesmith, M. T., & Bourgois, G. 1995, *JGR*, 100, 17069

Collier, M. R., Hamilton, D. C., Gloeckler, G., Bochsler, P., & Sheldon, R. B. 1996, *Geophys. Res. Lett.*, 23, 1191

Cranmer, S. R., & van Ballegooijen, A. A. 2003, *ApJ*, 594, 573

Cranmer, S. R. 2000, *ApJ*, 532, 1197

Cranmer, S. R. et al. 1999, *ApJ*, 511, 481,

Cranmer, S. R., Field, G. B., & Kohl, J. L. 1999, *ApJ*, 518, 937

David, C., Gabriel, A. H., Bely-Dubau, F., Fludra, A., Lemaire, P., & Wilhelm, K. 1998, *A&A*, 336, L90

Doschek, G. A., & Feldman, U. 1977, *ApJ*, 212, L143

Doschek, G. A., Warren, H. P., Laming, J. M., Mariska, J. T., Wilhelm, K., Lemaire, P., Schühle, U., & Moran, T. G. 1997, *ApJ*, 482, L109

Doschek, G. A., Feldman, U., Laming, J. M., Schühle, U., & Wilhelm, K. 2001, *ApJ*, 546, 559

Esser, R., & Edgar, R. J. 2000, *ApJ*, 532, L71,

Esser, R., & Edgar, R. J. 2001, *ApJ*, 563, 1062,

Feldman, W. C., Asbridge, J. R., Bame, S. J., Montgomery, M. D., & Gary, S. P. 1975, *JGR*, 80, 4181

Feldman, W. C., Barraclough, B. L., Phillips, J. L., & Wang, Y.-M. 1996, *A&A*, 316, 355

Gabriel, A. H., Bely-Dubau, F., & Lemaire, P. 2003, *ApJ*, 589, 623

Geiss, J., et al. 1995, *Science*, 268, 1033

Giordano, S., Antonucci, E., Noci, G., Romoli, M., & Kohl, J. L. 2000, *ApJ*, 531, L79

Grall, R. R., Coles, W. A., Spangler, S. R., Sakurai, T., & Harmon, J. K. 1997, JGR, 102, 263

Gringauz, K. I., et al. 1986, *Nature*, 321, 282

Hasegawa, A., Mima, K., & Duong-van, M. 1985, *Phys. Rev. Lett.*, 54, 2608

Hassler, D. M., Dammasch, I. E., Lemaire, P., Brekke, P., Curdt, W., Mason, H. E., Vial, J.-C., & Wilhelm, K. 1999, *Science*, 283, 810

Karney, C. F. F. 1978., *Phys. Fluids*, 21, 1584

Keenan, F. P., Kingston, A. E., Dufton, P. L., Doyle, J. G., & Widing, K. G. 1984, *Solar Physics*, 94, 91

Keenan, F. P. 1984, *Solar Physics*, 91, 27

Klimov, S. S., et al. 1986, *Nature*, 321, 292

Ko, Y.-K., Fisk, L. A., Geiss, J., Gloeckler, G., & Guhathakurta, M. 1997, *Solar Physics*, 171, 345

Krasnosel'skikh, V. V., Kruchina, E. N., Thejappa, G., & Volokitin, A. S. 1985, *A&A*, 149, 323

Laming, J. M. 2001a, *ApJ*, 546, 1149

Laming, J. M. 2001b, *ApJ*, 563, 828

Laming, J. M., & Feldman, U. 2003, *ApJ*, 591, 1257

Laming, J. M., & Grun, J. 2002, *Phys. Rev. Lett.*, 89, 125002

Laming, J. M., & Grun, J. 2003, *Physics of Plasmas*, 10, 1614

Laming, J. M., & Hwang, U. 2003, *ApJ*, 597, 347

Landi, E., Doron, R., Feldman, U., & Doschek, G. A. 2001, *ApJ*, 556, 912

Lennon, M., Bell, K. L., Gilbody, H. B., Hughes, J. G., Kingston, A. E., Murray, M. J., & Smith, F. J. 1988, *J. Phys. Chem. Ref. Data*, 17, 1285

Li, X. 2003, *A&A*, 406, 345

Luo, Q. Y., Wei, F. S., & Feng, X. S. 2003, *ApJ*, 584, 497

Markovskii, S. A. 2001, *ApJ*, 557, 337

Marsch, E., Pilipp, W. G., Thieme, K. M., & Rosenbauer, H. 1989, *JGR*, 94, 6893

Marsch, E. 1991, in *Physics of the Inner Heliosphere*, ed. R. Schwenn & E. Marsch, (Berlin: Springer), 45

Mazzotta, P., Mazzitelli, G., Colafrancesco, S., & Vittorio, N. 1998, *A&AS*, 133, 403

McClements, K. G., Dendy, R. O., Bingham, R., Kirk, J. G., & Drury, L. O’C. 1997, *MNRAS*, 291, 241

Moores, D. L., Golden, L. B., & Sampson, D. H. 1980, *J. Phys. B*, 13, 385

Neugebauer, M., Goldstein, B. E., Smith, E. J., & Feldman, W. C. 1996, *JGR*, 101, 17047

Ofman, L., Romoli, M., Poletto, G., Noci, G., & Kohl, J. L. 1997, *ApJ*, 491, L111

Ofman, L., & Davila, J. M. 2001, *ApJ*, 553, 935

Pariev, V. I., & Blackman, E. G. 2003, *MNRAS*, submitted, astro-ph/0310167

Patsourakos, S., & Vial, J.-C. 2000, *A&A*, 359, L1

Quataert, E. 2003, *MNRAS*, submitted, astro-ph/0308451

Reisenfeld, D. B., Gary, S. P., Gosling, J. T., Steinberg, J. T., McComas, D. J., Goldstein, B. E., & Neugebauer, M. 2001, *JGR*, 106, 5693

Salem, C., Hubert, D., Lacombe, C., Bale, S. D., Mangeny, A., Larson, D. E., & Lin, R. P. 2003, *ApJ*, 585, 1147

Savin, D. W., & Laming, J.M. 2002, *ApJ*, 566, 1166

Schwartz, S. J., Feldman, W. C., & Gary, S. P. 1981, *JGR*, 86, 4574

Shapiro, V. D., Bingham, R., Dawson, J. M., Dobe, Z., Kellett, B. J., & Mendis, D. A. 1999, *JGR*, 104, 2537

Shull, J. M., & van Steenberg, M. 1982, *ApJS*, 48, 95

Summers, H. P., & McWhirter, R. W. P., *J. Phys. B*, 12, 2387

Vaisberg, D. L., Galeev, A. A., Zastenker, G. N., Klimov, S. I., Nozdrachev, M. N., Sagdeev, R. Z., Sokolov, A. Y., & Shapiro, V. D. 1983, *Sov. Phys. JETP*, 58, 716

Vocks, C., & Mann, G. 2003, ApJ, 593, 1134

von Steiger, R., et al. 2000, JGR, 105, 27217

Wilhelm, K., Marsch, E., Dwivedi, B., Hassler, D. M., Lemaire, P., Gabriel, A. H., & Huber, M. C. E. 1998, ApJ, 500, 1023

Wilhelm, K., Dommisch, I. E., Marsch, E., & Hassler, D. M. 2000, A&A, 353, 749

Woo, R., 1996, Nature, 379, 321

Woo, R., & Habbal, S. R. 1997, ApJ, 474, 39

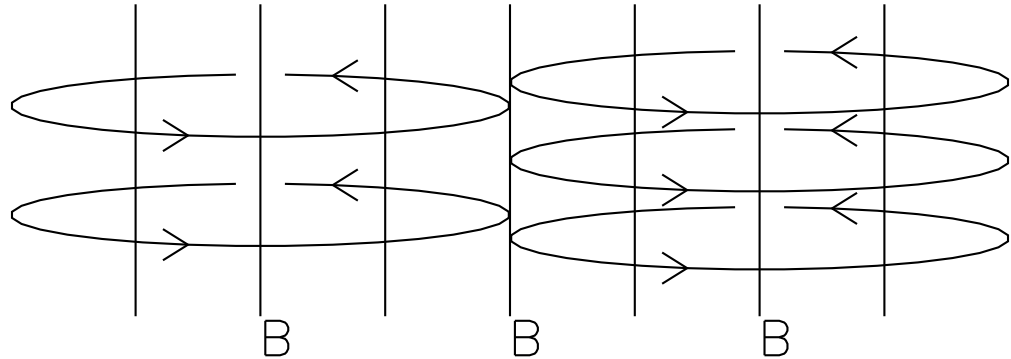


Fig. 1.— Schematic diagram illustrating the excitation of lower hybrid waves in a density gradient. The magnetic field direction is vertical, and density is increasing to the right. Gyrating ions can give a local anisotropy in the distribution function in the direction perpendicular to both of these vector, into or out of the page, when the characteristic length of the density gradient becomes comparable to the ion gyroradius.

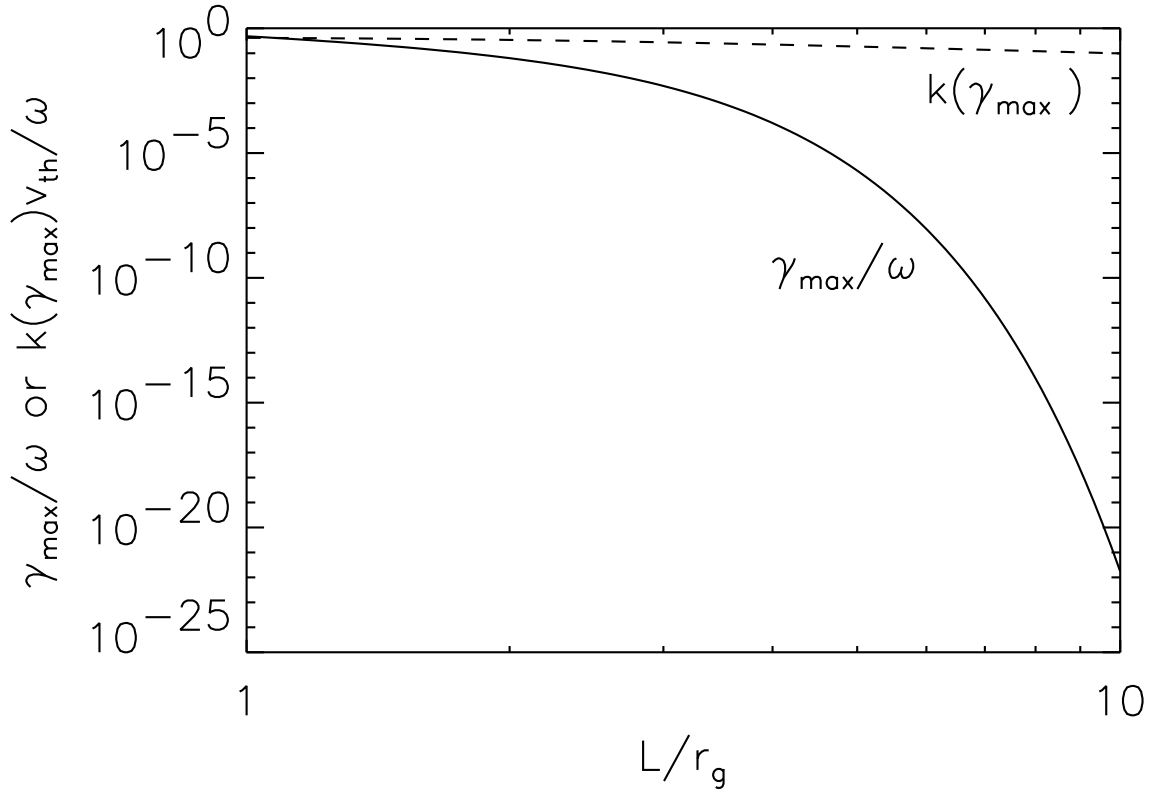


Fig. 2.— Plot of maximum lower-hybrid growth rate in units of the wave frequency γ_i/ω (the factor $Af q^2/M$ is omitted) and the wavevector where this maximum is found in units of $\omega/v_{th\perp}$ against the density scale length in units of the ion gyroradius L/r_g .

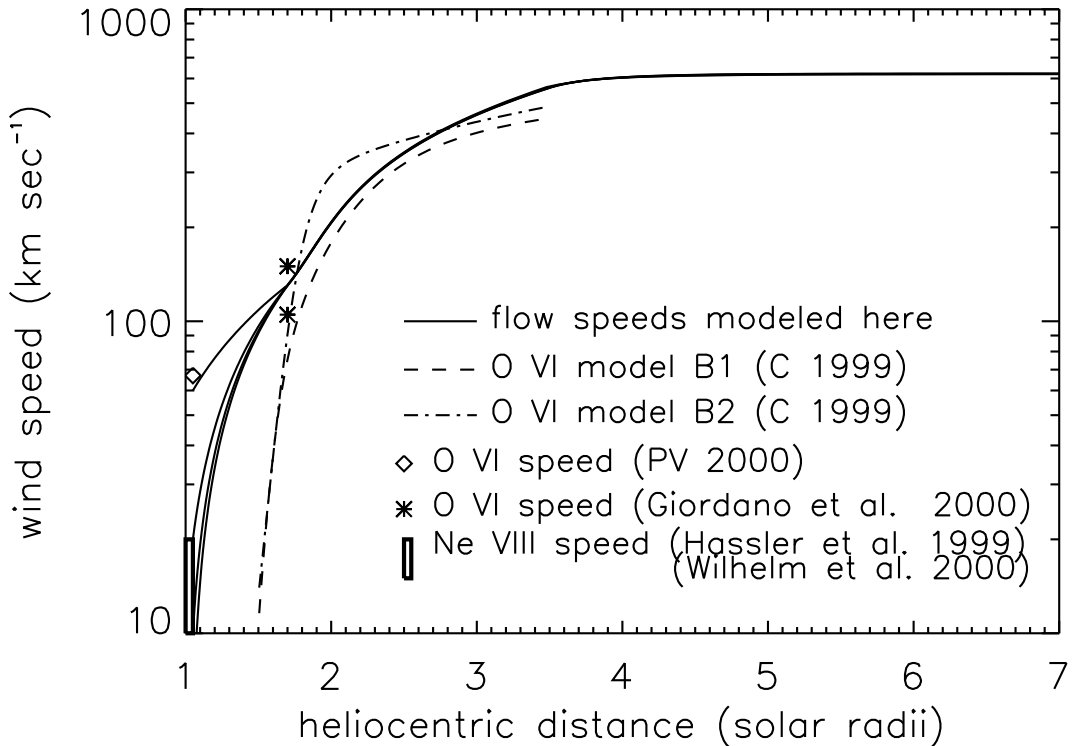


Fig. 3.— Plot of solar wind ion flow speeds adopted in the ionization models. For reference we also show models B1 and B2 from Cranmer et al. (1999), some flow speeds determined from O VI Doppler dimming observations by Patsourakos & Vial (2000), Giordano et al. (2000), and direct Doppler shift measurements by Hassler et al. (1999) and Wilhelm et al. (2000).

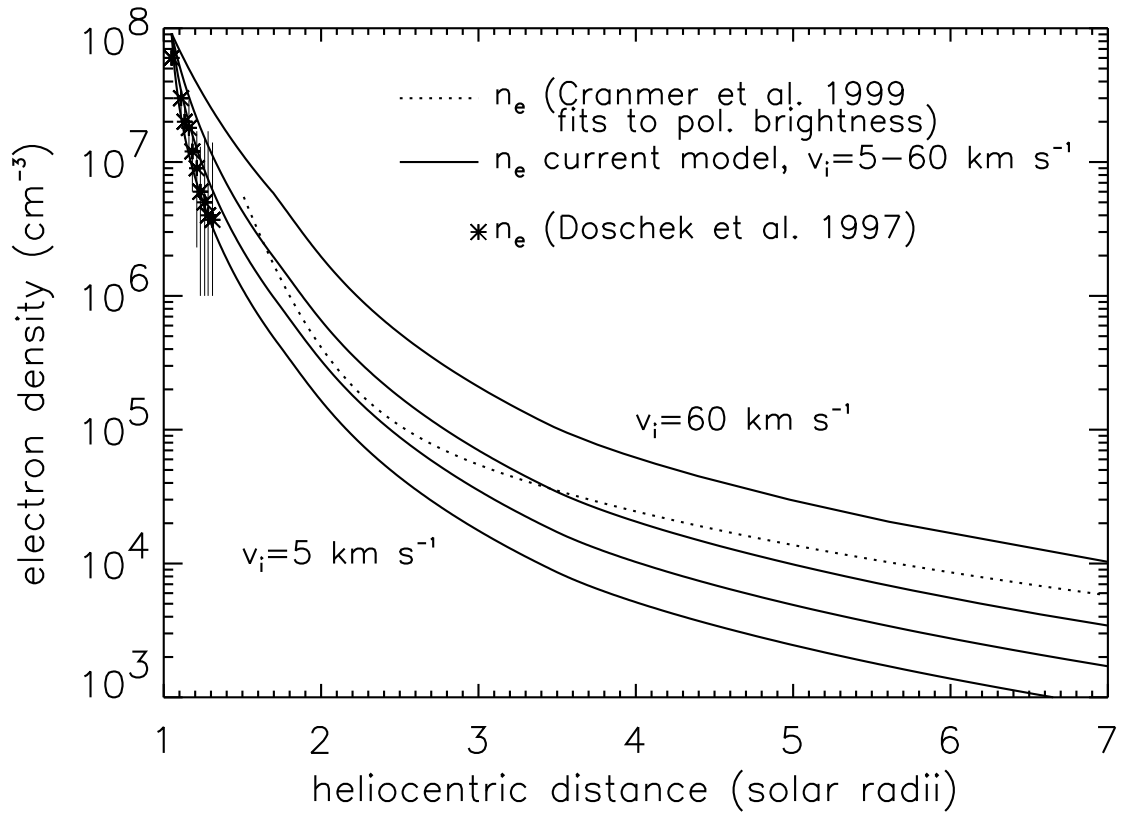


Fig. 4.— Plot of solar wind densities derived from the various models with different initial flow speeds, 5, 10, 20, and 60 km s⁻¹, increasing bottom to top. Densities derived from a diagnostic line ratio in Si VIII (Doschek et al. 1997) and polarization brightness (Cranmer et al. 1999) are given for comparison.

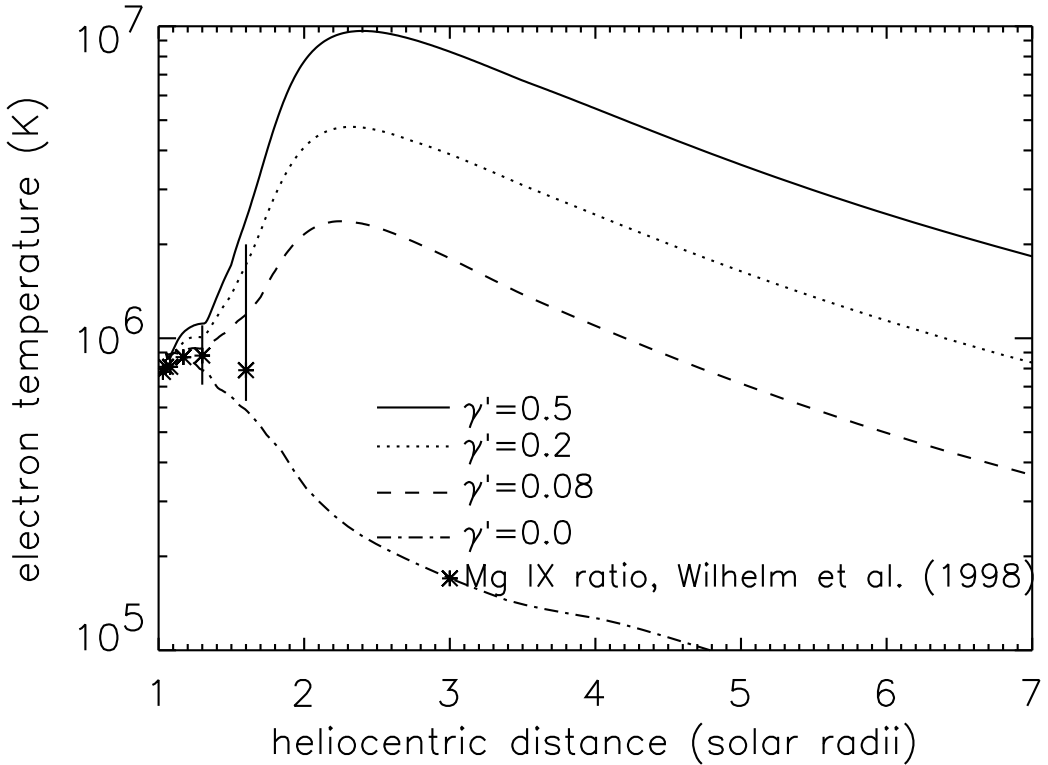


Fig. 5.— Plot of electron temperature variation with heliocentric distance for models with an initial flow speed of 10 km s^{-1} and varying degrees of collisionless ion-electron coupling, $\gamma' = (\gamma_i M_i / \omega A f q^2) (\omega / k v_{iy})^2$. Measurements from the Mg IX 706/750 temperature sensitive ratio by Wilhelm et al. (1998) are given for comparison. We have estimated error bars on their points for 1.3 and $1.6 R_\odot$ from the scatter of points given in their Fig. 8.

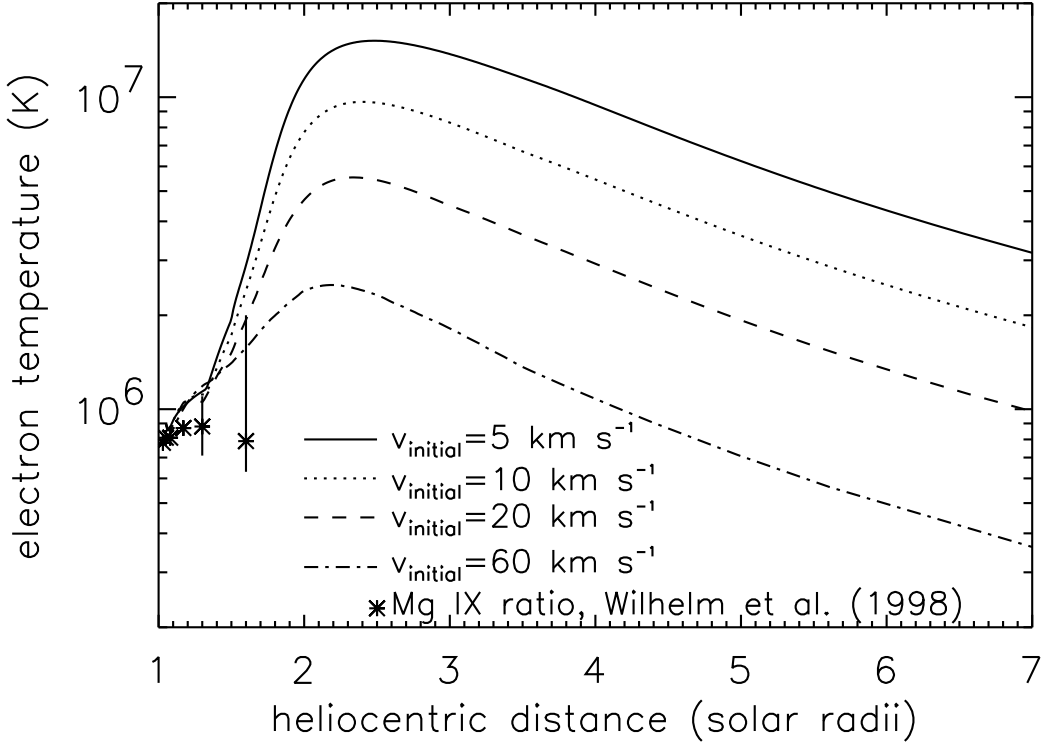


Fig. 6.— Plot of electron temperature variation with heliocentric distance for models with $\gamma' = (\gamma_i M_i / \omega A f q^2) (\omega / k v_{iy})^2 = 0.5$ and initial flow speeds varying in the range $5-60 \text{ km s}^{-1}$. Measurements from the Mg IX 706/750 temperature sensitive ratio by Wilhelm et al. (1998) are given for comparison. We have estimated error bars on their points for 1.3 and $1.6 R_\odot$ from the scatter of points given in their Fig. 8.

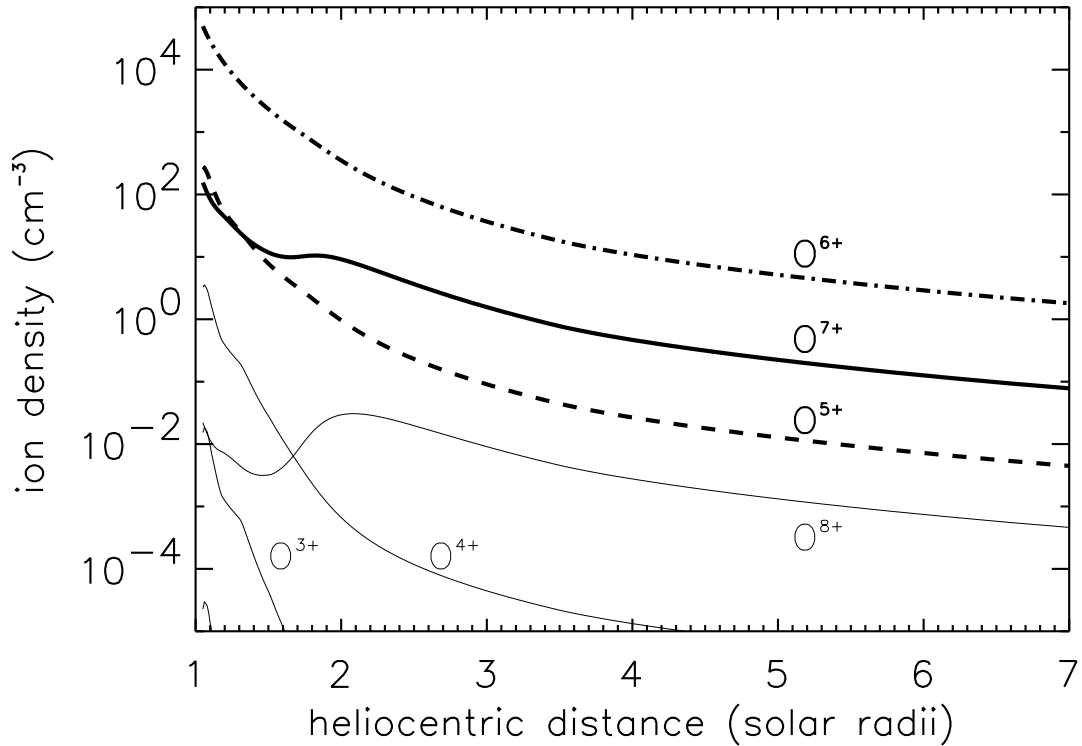


Fig. 7.— Plot of the evolution of the O ionization balance with heliocentric distance for initial flow speed 20 km s^{-1} and $(\gamma_i M_i / \omega A f q^2) (\omega^2 / k^2 v_{iy}^2) = 0.5$, corresponding to $L/r_g \simeq 2$. The initial ionization balance corresponds to the coronal hole electron temperature of $9 \times 10^5 \text{ K}$. Increased ionization starts at about $1.5 R_\odot$, as ion-electron energy transfer increases in response to the strong ion cyclotron heating at this location. Charge states are frozen in beyond a distance of $2-2.5 R_\odot$, and correspond to those measured in situ by Ulysses.

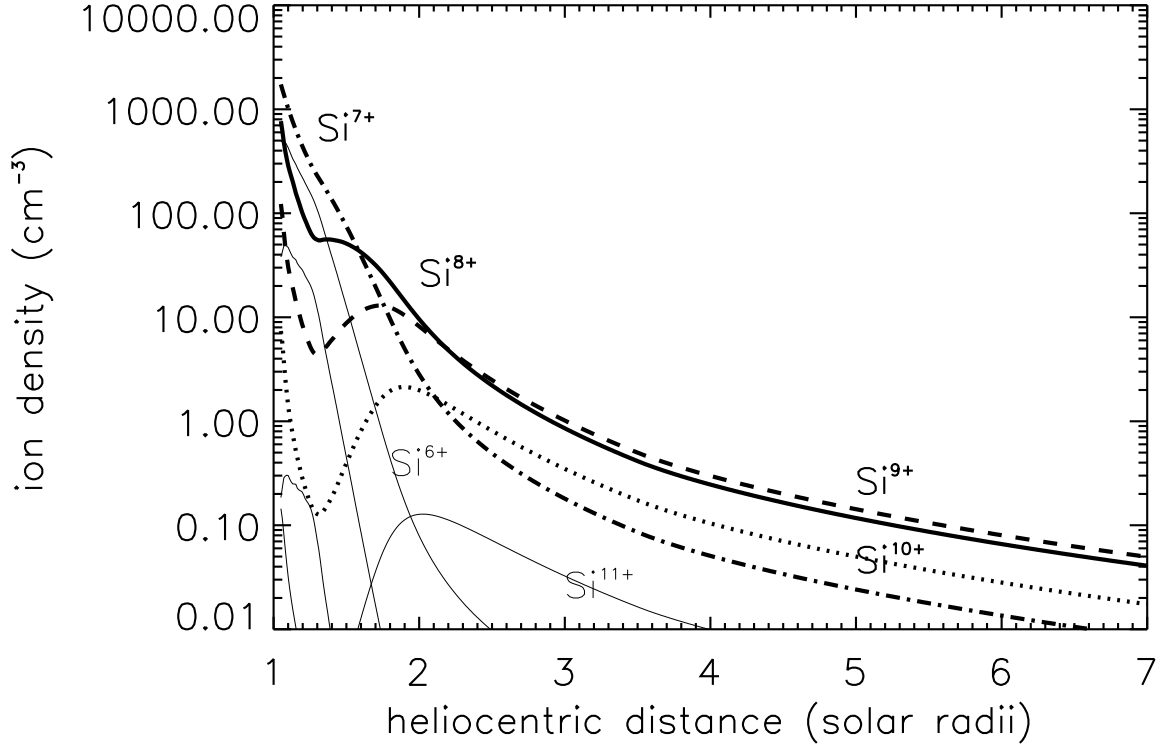


Fig. 8.— Plot of the evolution of the Si ionization balance with heliocentric distance for initial flow speed 20 km s^{-1} and $(\gamma_i M_i / \omega A f q^2) (\omega^2 / k^2 v_{iy}^2) = 0.5$, corresponding to $L/r_g \simeq 2$. The initial ionization balance corresponds to the coronal hole electron temperature of $9 \times 10^5 \text{ K}$. Increased ionization starts at about $1.5 R_\odot$, as ion-electron energy transfer increases in response to the strong ion cyclotron heating at this location. Charge states are frozen in beyond a distance of $2-2.5 R_\odot$, and correspond to those measured in situ by Ulysses.

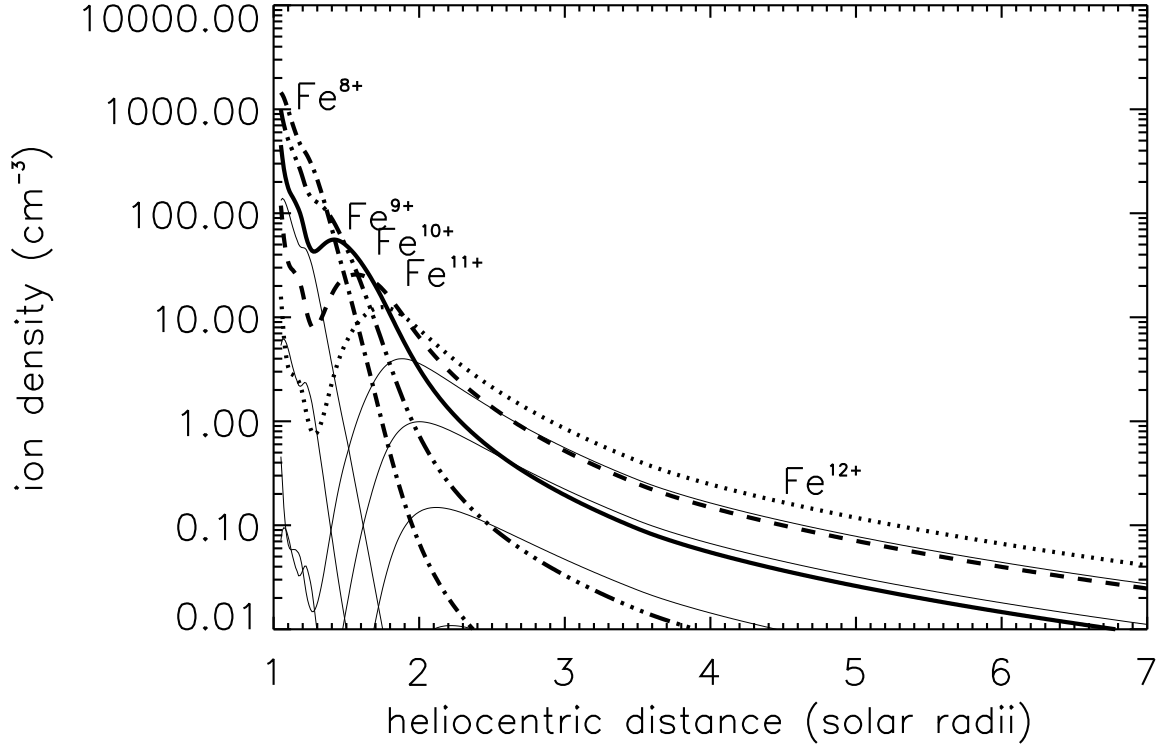


Fig. 9.— Plot of the evolution of the Fe ionization balance with heliocentric distance for initial flow speed 20 km s^{-1} and $(\gamma_i M_i / \omega A f q^2) (\omega^2 / k^2 v_{iy}^2) = 0.5$, corresponding to $L/r_g \simeq 2$. The initial ionization balance corresponds to the coronal hole electron temperature of $9 \times 10^5 \text{ K}$. Increased ionization starts at about $1.5 R_\odot$, as ion-electron energy transfer increases in response to the strong ion cyclotron heating at this location. Charge states are frozen in beyond a distance of $2-2.5 R_\odot$, and correspond to those measured in situ by Ulysses.

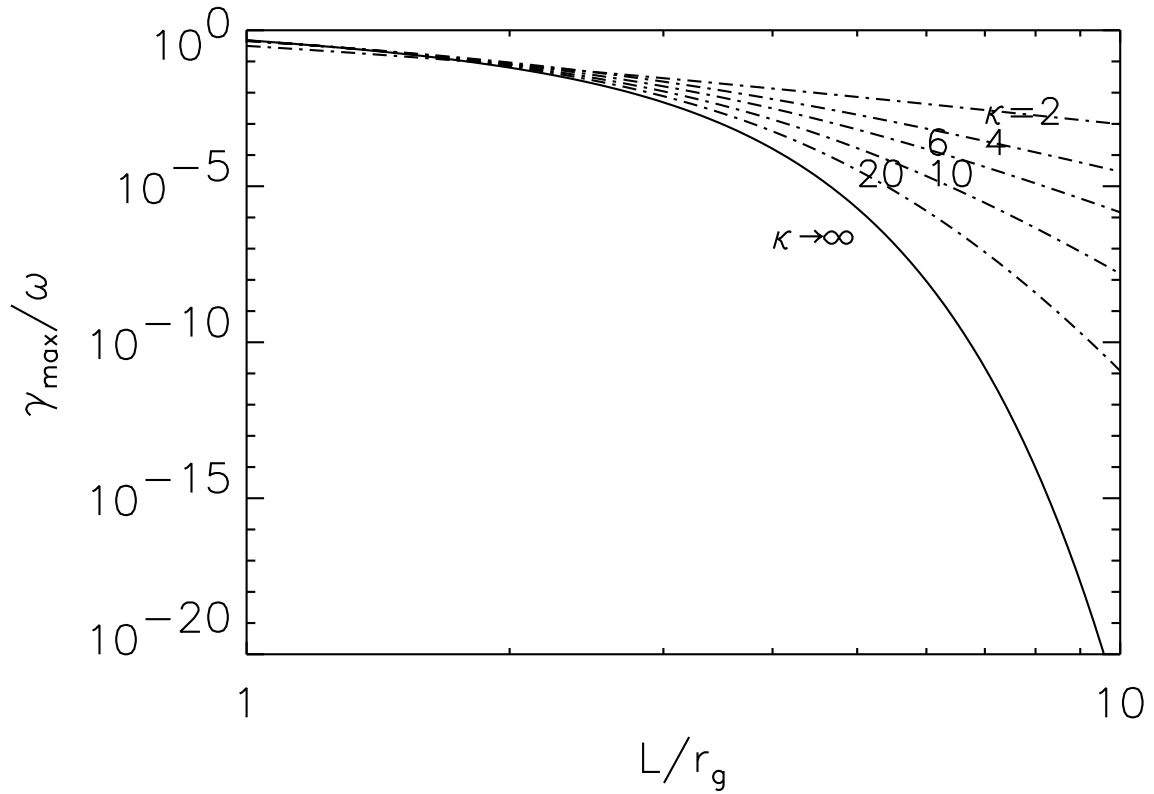


Fig. 10.— Plot of maximum lower-hybrid growth rate in units of the wave frequency $\gamma_i M_i / \omega A f q^2$ against the density scale length in units of the ion gyroradius L/r_g , for Maxwellian $\kappa \rightarrow \infty$ and $\kappa = 2, 4, 6, 10$, and 20 .

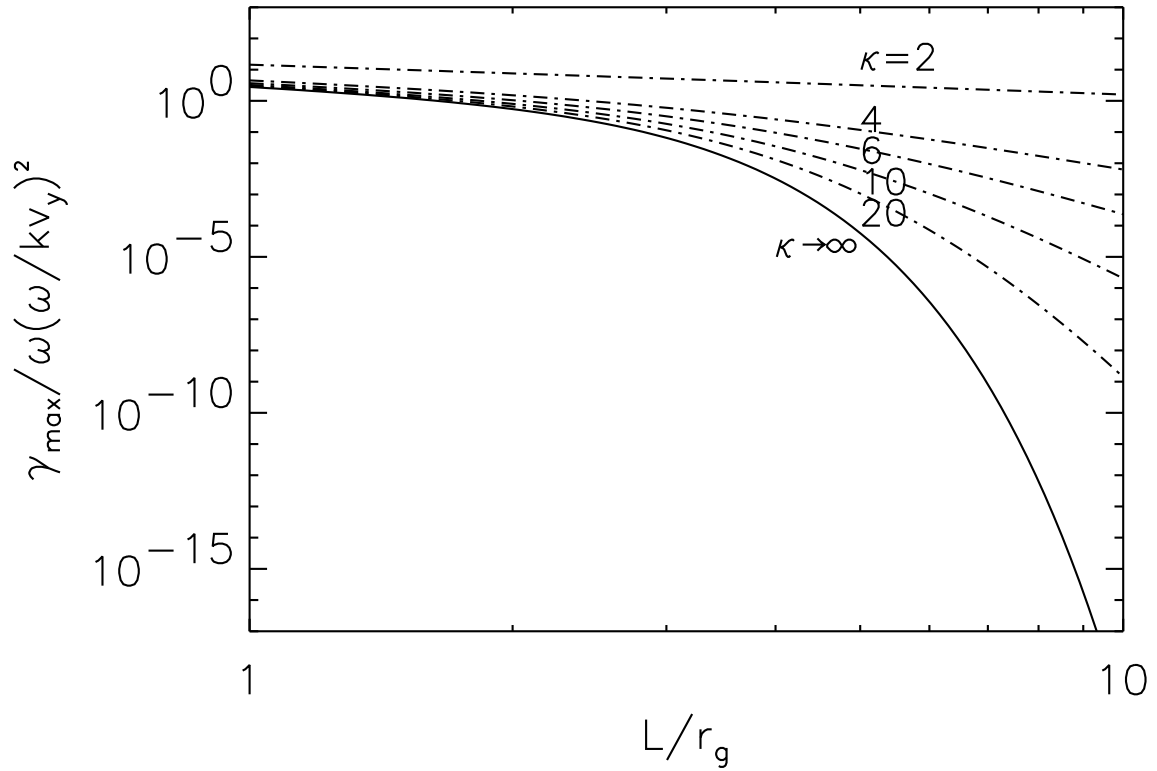


Fig. 11.— Plot of $\gamma' = (\gamma_i M_i / \omega A f q^2) (\omega / kv_{iy})^2$ in units of the wave frequency against the density scale length in units of the ion gyroradius L/r_g , for Maxwellian $\kappa \rightarrow \infty$ and $\kappa = 2, 4, 6, 10$, and 20.

Table 1. C and O Ionization Fractions.

v_{start} km s $^{-1}$	γ'	C^{4+}/C^{5+}	C^{5+}/C^{6+}	O^{6+}/O^{7+}
2.5	0.0	0.86	9.0	375
2.5	0.048	0.82	8.4	100
2.5	0.2	0.78	7.7	50
2.5	0.5	0.74	7.2	35
2.5	1.0	0.64	6.4	24
5	0.0	0.84	8.9	361
5	0.08	0.81	8.4	148
5	0.2	0.71	7.3	46
5	0.5	0.63	6.3	24
5	1.0	0.57	5.7	18
10	0.0	0.80	8.7	340
10	0.08	0.80	8.6	282
10	0.2	0.68	7.3	65
10	0.5	0.53	5.5	20
10	1.0	0.45	4.5	12
20	0.0	0.76	8.4	317
20	0.08	0.77	8.5	334
20	0.2	0.69	7.7	141
20	0.5	0.48	5.5	25
20	1.0	0.35	3.7	11
60	0.0	0.68	7.9	259
60	0.08	0.67	7.8	257
60	0.2	0.64	7.6	222
60	0.5	0.51	6.2	73
60	1.0	0.31	3.8	28
Geiss et al. (1995)		0.42	5.0	30
Ko et al. (1997)		0.48	5.3	32

Table 2. Mg Ionization Fractions ($\gamma' = 0.5$).

v_{start} km s $^{-1}$	Mg^{6+}	Mg^{7+}	Mg^{8+}	Mg^{9+}	Mg^{10+}
2.5	0.053	0.31	0.45	0.14	0.043
5	0.036	0.26	0.47	0.18	0.052
10	0.012	0.16	0.49	0.27	0.073
20	0.006	0.11	0.47	0.32	0.090
60	0.006	0.10	0.48	0.32	0.088
Ko et al. (1997)	0.028	0.12	0.23	0.23	0.40

Table 3. Si Ionization Fractions ($\gamma' = 0.5$).

v_{start} km s $^{-1}$	Si $^{7+}$	Si $^{8+}$	Si $^{9+}$	Si $^{10+}$	Si $^{11+}$
2.5	0.36	0.43	0.15	0.019	0.001
5	0.24	0.45	0.24	0.045	0.003
10	0.12	0.40	0.37	0.10	0.009
20	0.068	0.34	0.43	0.15	0.015
60	0.095	0.38	0.40	0.11	0.007
Geiss et al. (1995)	0.08	0.31	0.41	0.19	0.01
Ko et al. (1997)	0.056	0.21	0.43	0.23	0.054

Table 4. Fe Ionization Fractions ($\gamma' = 0.5$).

v_{start} km s $^{-1}$	Fe $^{9+}$	Fe $^{10+}$	Fe $^{11+}$	Fe $^{12+}$	Fe $^{13+}$	Fe $^{14+}$
2.5	0.30	0.34	0.19	0.06	0.009	0.001
5	0.14	0.30	0.30	0.18	0.049	0.009
10	0.034	0.15	0.28	0.31	0.16	0.050
20	0.012	0.077	0.21	0.35	0.23	0.095
60	0.023	0.11	0.26	0.37	0.18	0.051
Geiss et al. (1995)	0.04	0.17	0.28	0.26	0.16	0.05
Ko et al. (1997)		0.16	0.25	0.28	0.16	